Gait Design for a Snake Robot by Connecting Curve Segments and Experimental Demonstration

doi: 10.1109/TRO.2018.2830346

Gait Design for a Snake Robot by Connecting Curve Segments and Experimental Demonstration

Tatsuya Takemori, *Student Member, IEEE,* Motoyasu Tanaka, *Member, IEEE,* and Fumitoshi Matsuno, *Member, IEEE,*

***Abstract*—This paper presents a method for designing the gait of a snake robot that moves in a complicated environment. We propose a method for expressing the target form of a snake robot by connecting curve segments whose curvature and torsion are already known. Because the characteristics of each combined shape are clear, we can design the target form intuitively and approximate a snake robot configuration to this form with low computational cost. In addition, we propose two novel gaits for the snake robot as a design example of the proposed method. The first gait is aimed at moving over a flange on a pipe, while the other is the crawler gait aimed at moving over rough terrain. We demonstrated the effectiveness of the two gaits on a pipe and rough terrain in experiments.**

***Index Terms*—Snake Robot, Redundant Robots, Search and Rescue Robots, and Inspection.**

I. Introduction

A Snake robot is expected to perform a wide variety of tasks while having a simple structure, and control method of the snake robot have been extensively studied. The ultimate goal of the present study is to realize a snake robot that can move in any environment.

A control method that converges the controlled variable to the target value using a model has been proposed. Two models are used for this method, namely a friction model(e.g. [1]) and a model that considers the nonholonomic constraint(e.g. [2]). Such a method using a model of the interaction between the snake robot and environment is effective for a simple environment such as a plane. However, the method cannot be applied to an unknown irregular environment.

Therefore, a method that realizes functions also in an irregular environment by devising the whole form of a snake robot has been proposed. Although such a method does not involve kinematic or dynamic optimization, it is easy to apply to a complicated environment that cannot be modeled. As a method of controlling the whole form of the snake robot, various gaits, such as *sidewinding* and *lateral rolling*, have been realized by defining the trajectory of the joint angle as a parameterized equation [3], [4]. Using the parameterized equation, we can control the form of the snake robot with several gait parameters whose physical meanings are clear. However, when the target form of the snake robot becomes more complicated, it is difficult to directly formulate the joint angles that realize that shape.

Without using a gait function, a method of approximating a discrete snake robot to a continuous spatial curve that is called the *backbone curve* [5] and expresses a target form of a snake robot has been studied [6]–[11]. Employing this method, it is possible to consider a snake robot as a continuous curve abstractly and there is no need to directly decide the joint angles, and it is thus easy to design a complicated shape. In [5]–[7], a method for deriving joint angles to approximate the robot configuration to the backbone curve was proposed. Andersson [6] proposed a method of matching the link connection points on the target curve for a multi-link robot having joints with two degrees of freedom. However, in the case that each joint has only one degree of freedom, it is impossible in principle to match all the connection points with the curve and the method cannot be applied. Yamada et al. modeled the form of the snake robot using the Frenet–Serret formulas [8], and proposed a method of deriving suitable joint angles based on the curvature and torsion of the target curve [7]. Furthermore, adaptation to the environment has been realized [9] by combining torque feedback with motion planning using this approximation method. Because Yamada's approximate method [7] can be easily applied when the curvature and torsion of the target curve are easily obtained, we apply this method. Kamegawa [10] realized *bending helical rolling* whose target form is generated by connecting a helix and a shape called the *bending helix* for propulsion on a bending pipe. Zhen et al. [11] proposed a *rolling hump* whose target form is a curve obtained by superposing hump-shaped curves and an arc-shaped curve, and made it possible for a snake robot to climb over an obstacle on the ground. In [10], [11], the curvature and torsion were calculated from the continuous curve as the target form, and the target joint angles were obtained using Yamada's method [7].

However, it is difficult to analytically express an appropriate continuous curve when a more complicated target form is required. In addition, the torsion may diverge to infinity in some cases that there is a region where the curvature is zero on the curve [8], and the corresponding target joint angle cannot then be calculated using Yamada's method. We, therefore, propose in this paper a method of designing the target form by connecting *curve segments* whose characteristics are already known, so that the target form can be intuitively designed and curvature and torsion are easy to be calculated. In addition to simple shapes, such as straight lines, arcs, and helixes, any shape can be used as a *curve segment* as long as the curvature and torsion are known. If simply connecting shapes, Yamada's method [7] cannot be applied owing to the discontinuous twist of the connecting part of curve segments. In our proposed method, this problem is solved by formulating the twist of the connecting part, and it is also possible to treat the twist as if it is a virtual roll joint. In addition, we propose two novel gaits of a snake robot designed with our proposed method. These gaits allow movement in a complex environment. One gait makes it possible to climb over a flange on a pipe. The other gait is the crawler gait that allows the snake robot to move over rough terrain.

This research is based on [12] and is improved by adding the generalization of connected shapes, deriving shape constraints, proposing turning and recovery motion of the crawler gait, and conducting experiments.

II. Shape Fitting Using the Backbone Curve

We use the snake robot model composed of alternately connected pitch-axis and yaw-axis joints as shown in Fig. 1. All links have a length of l, the number of joints is n_{joint}, and the i-th relative joint angle is θ_i. The upper value of an absolute angle of joint is $\theta_{\max}$

This work was partially supported by the ImPACT Program of the Council for Science, Technology and Innovation (Cabinet Office Government of Japan).

T. Takemori and F. Matsuno are with the Department of Mechanical Engineering and Science, Graduate School of Engineering, Kyoto University, Kyoto, 606-8501, Japan (e-mail: takemori.tatsuya.23a@st.kyoto-u.ac.jp, matsuno@me.kyoto-u.ac.jp).

M. Tanaka is with the Department of Mechanical and Intelligent Systems Engineering, The University of Electro-Communications, Tokyo 182-8585, Japan (e-mail: mtanaka@uec.ac.jp).

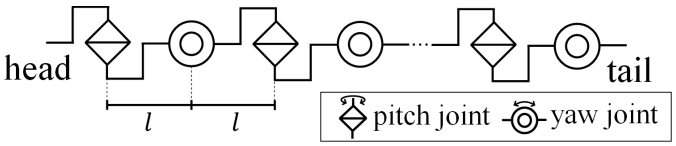

Fig. 1. Structure of a snake robot.

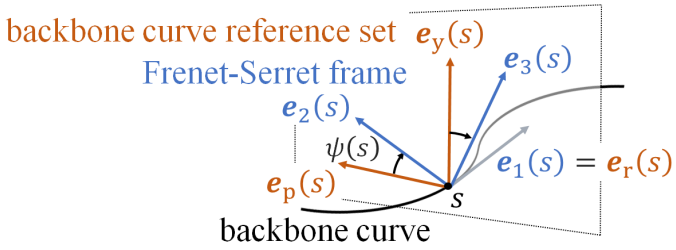

Fig. 2. Difference between the Frenet–Serret frame and backbone curve reference set.

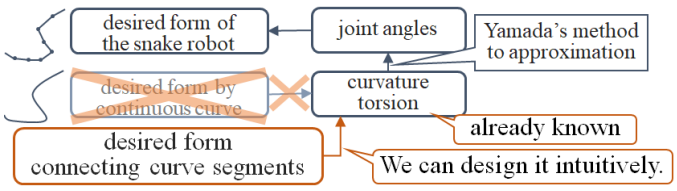

Fig. 3. Overview of the proposed method.

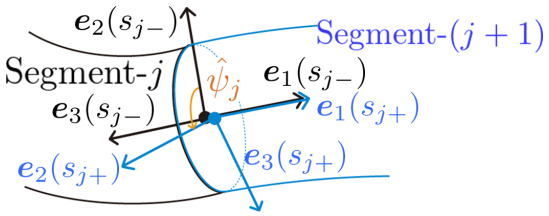

Fig. 4. Joint of segments.

and the angle of each joint can be independently controlled within the range $|\theta_i| \leq \theta_{\max}$. The present paper uses only this model but the method described in Section III can also be applied to a snake robot having other joint configurations by following [7].

We used Yamada's method [7] to calculate the joint angles and approximate a snake robot to the target form, because it has a low computational cost and is easily applied when the curvature and torsion of a target form are known.

In Fig. 2, $\boldsymbol{e}_1(s), \boldsymbol{e}_2(s)$, and $\boldsymbol{e}_3(s)$ are unit vectors forming the orthonormal basis, called *the Frenet–Serret frame*. s is the variable of length along the curve. $\boldsymbol{e}_1(s)$ is a vector tangential to the curve at s, $\boldsymbol{e}_2(s)$ is a vector that indicates the direction of change in the curve at s, and $\boldsymbol{e}_3(s)$ is given by $\boldsymbol{e}_1(s) \times \boldsymbol{e}_2(s)$. This coordinate system depends on the shape of the curve. In contrast with the Frenet–Serret model, it is necessary to consider the joint direction to model a snake robot. As shown in Fig. 2, a *backbone curve reference set* $\boldsymbol{e}_r(s)$, $\boldsymbol{e}_p(s)$, and $\boldsymbol{e}_y(s)$ is defined on the curve by regarding a snake robot as a continuous curve. $\boldsymbol{e}_r(s)$ is equal to $\boldsymbol{e}_1(s)$. $\boldsymbol{e}_p(s)$ and $\boldsymbol{e}_y(s)$ are unit vectors respectively oriented along the pitch axis and yaw axis at s. These vectors are referred to as the basis vectors of *the backbone curve reference set* that is determined by the orientation of each part of the robot.

As shown in Fig. 2, the twist angle of the Frenet–Serret frame and the backbone curve reference set around $\boldsymbol{e}_1(s)$ is denoted $\psi(s)$, which can be obtained as

$$\psi(s) \quad = \quad \int_0^s \tau(\hat{s})\mathrm{d}\hat{s} + \psi(0), \tag{1}$$

where $\psi(0)$ is an arbitrary integral constant corresponding to the initial angle. By changing $\psi(0)$, the entire backbone curve reference set rotates around the curve and a rolling motion is generated. Here $\kappa(s)$ and $\tau(s)$ are the curvature and torsion in the Frenet–Serret formulas, and $\kappa_p(s)$ and $\kappa_y(s)$ are then respectively the curvatures around the pitch axis and yaw axis in the backbone curve reference set and obtained as

$$\kappa_p = -\kappa(s)\sin\psi(s), \ \kappa_y = \kappa(s)\cos\psi(s). \tag{2}$$

Finally, the target angle of each joint is calculated as

$$\theta_i^d = \begin{cases} \int_{s_\mathrm{h}+(i-1)l}^{s_\mathrm{h}+(i+1)l} \kappa_p(s)\mathrm{d}s & (i:\text{odd}) \\ \int_{s_\mathrm{h}+(i-1)l}^{s_\mathrm{h}+(i+1)l} \kappa_y(s)\mathrm{d}s & (i:\text{even}) \end{cases}, \tag{3}$$

where s_h is the head position of the snake robot on a target continuous curve. The robot can change its shape smoothly with *shift control*, that changes s_h and thus the region corresponding to the body of the robot in the target curve.

III. Backbone Curve Connecting Curve Segments

It is difficult to represent a complex target form of a snake robot analytically. There is also the problem that torsion sometimes becomes infinit if some part of the target form includes a region of zero curvature [8]. To solve these problems, we proposed a method in which the target form is represented by connecting curve segments. In addition to segments having the simplest three shapes of a straight line, a circular arc, and a helix, curve segments of any shape can be used as long as the curvature and torsion are known. Using this method, we can intuitively design the target form as a combination of curve segments whose geometric properties are clear. Moreover, the corresponding joint angle is easily calculated because the curvature and torsion are known. We call a curve segment connected employing this method a *segment*, and describe how to configure the target form by connecting segments.

A. Form Configuration Obtained by Connecting Segments

An overview of our approach is shown in Fig. 3, while the approximation method is described in Section II. There is no problem with the approximation method for internal parts of segments because the curvature and torsion of each segment are already known. However, because the Frenet–Serret frame is discontinuous at the *connection part* where segments are connected, it is necessary to devise a representation. Counting from the head, the j-th segment is referred to as *segment* $j (j \in \mathbb{Z})$. $s = s_j$ is the point of connection part j connecting segment j and $(j+1)$. The length l_j of segment j, satisfies the relation

$$s_j = s_{j-1} + l_j. \tag{4}$$

Segments j and $(j+1)$ must be in contact with each other at $s = s_j$. The state of connection part j is shown in Fig. 4. s_{j-} and s_{j+} are the points at an infinitesimal distance before and after connection part j, respectively. The Frenet–Serret frame, curvature, and torsion at s_j are represented by those at s_{j-}.

The curvature and torsion of segment j are denoted $\kappa_j(s)$ and $\tau_j(s)$, respectively. The point $s = 0$ in $\kappa_j(s)$ and $\tau_j(s)$ is the beginning point of segment j. The curvature of the target form $\kappa(s)$ and the torsion $\tau(s)$ can be obtained as

$$\kappa(s) = \kappa_j(s - s_{j-1}) \qquad (s_{j-1} < s \leq s_j) \tag{5}$$

$$\tau(s) = \tau_j(s - s_{j-1}) \qquad (s_{j-1} < s \leq s_j). \tag{6}$$

TABLE I
CHARACTERISTICS OF EACH TYPE OF SIMPLE SHAPE SEGMENT

type	curvature κ_j	torsion τ_j	length l_j
helix	$a_j/(a_j^2+b_j^2)$	$b_j/(a_j^2+b_j^2)$	$\phi_i\sqrt{a_j^2+b_j^2}$
circular arc	$1/r_j$	0	$\phi_j r_j$
straight line	0	0	l_j

In Frenet–Serret formulas, $\kappa(s)$ is defined as being positive, but (2) can be used even if $\kappa(s)$ is negative. The curve bends in the direction opposite $\boldsymbol{e}_2(s)$ in the region where $\kappa(s) < 0$.

We next consider the twist at the connection part. As shown in Fig. 4, the angle between $\boldsymbol{e}_2(s_{j-})$ and $\boldsymbol{e}_2(s_{j+})$ around $\boldsymbol{e}_1(s_{j-})$ is denoted $\hat{\psi}_j$. $\hat{\psi}_j$ is the twist angle, and is one of the design parameters. To consider this twist in the calculation of the approximation method, (1) must be replaced by

$$\psi(s) \quad = \quad \int_0^s \tau(\hat{s})\mathrm{d}\hat{s} + \psi(0) + \sum_j \hat{\psi}_j u(s - s_j), \qquad (7)$$

where $u(s)$ is the step function which is 0 if $s < 0$ and 1 if $s \geq 0$. The joint angles of the snake robot can therefore be obtained using (2), (3), (5), (6), and (7). To design a target form, we have to determine the shape of each segment and the twist angle $\hat{\psi}_j$. By changing $\hat{\psi}_j$, we can change the target form as if there is a virtual roll axis joint of the snake robot at the connection part of the target form.

B. Characteristics of Shapes

The shapes of the connected curve segments are classified into simple shapes and other shapes. Shape examples of each type will be explained.

1) Simple Shapes: We first describe simple shapes for segments whose curvature and torsion are constant, namely a straight line, a circular arc, and a helix.

In the case of a straight line, the Frenet–Serret frame and torsion are not defined. In this study, we newly define these for a straight line to handle straight segments in the same way as other segments. The frame inside the straight line is defined as being equal to the frame at $s = s_{j-}$ and torsion is zero.

A circular arc, whose curvature is constant and torsion is zero, is defined by its radius r_j and central angle ϕ_j.

A helix (which is a normal helix in this paper) is a curve whose curvature and torsion have non-zero constant values. The radius a_j, slope b_j, and central angle ϕ_j define the shape of a helix. The helical pitch p_j (i.e., the height of a coil) is given as $b_j = p_j/2\pi$. α_j is the angle between the tangent of the helix and the plane perpendicular to the axis of the helix, and can be calculated as $\alpha_j = \arctan(b_j/a_j)$. $\boldsymbol{e}_2(s)$ is directed perpendicularly from each point of the helix to the axis of the helix. These characteristics are summarized in Table I.

2) Other Shapes: Even if curvature and torsion are not constant, any shape can be used as long as the curvature and torsion are known. For example, the curvature and torsion of a serpenoid curve used for the lateral undulation of a passive wheeled snake robot are

$$\kappa_j(s) = A\sin\{\omega(s - s_{\mathrm{offset}})\}, \tau_j(s) = 0, \qquad (8)$$

where A is the maximum curvature of the serpenoid curve, ω is the spatial frequency of the curve, and s_{offset} is the offset term representing the initial phase of the serpenoid curve.

C. Shape Constraints

Consider a shape constraint condition such that the target joint angle does not exceed $\theta_{\max}$. The upper limit of the absolute value of the curvature $\kappa_{\max}$ is determined as $\kappa_{\max} = \theta_{\max}/2l$. Consider the case that the shape is designed such that $\kappa(s)$ satisfies

$$|\kappa(s)| \leq \kappa_{\max}. \qquad (9)$$

In this case, (2) and (3) yield

$$\begin{aligned} |\theta_i^d| \quad &= \quad \begin{cases} |\int_{s_\mathrm{h}+(i-1)l}^{s_\mathrm{h}+(i+1)l} -\kappa(s)\sin\psi(s)\mathrm{d}s| & (i:\mathrm{odd}) \\ |\int_{s_\mathrm{h}+(i-1)l}^{s_\mathrm{h}+(i+1)l} \kappa(s)\cos\psi(s)\mathrm{d}s| & (i:\mathrm{even}) \end{cases} \\ &\leq \quad \int_{-l}^{l} |\kappa(s)|\mathrm{d}s \;=\; 2l\kappa_{\max} \;=\; \theta_{\max}. \end{aligned} \qquad (10)$$

We can then confirm that the absolute value of the target joint angle $|\theta_i^d|$ does not exceed $\theta_{\max}$.

However, (9) is the most conservative condition assuming that rolling motion occurs in the case that the integration range of (3) is totally within a circular arc of the curvature $\kappa_{\max}$. Because the segments contained in the integral range vary owing to the change in the target form or shift control, it is difficult to consider optimal constraint conditions in all states including the case of $s_\mathrm{h} + (i-1)l < s_j < s_\mathrm{h} + (i+1)l$; i.e., the case that the integration range in (3) includes multiple segments. This paper therefore designs the form according to the condition (9).

D. Fitting Accuracy

In this paper, we formulate the discontinuous twist at the connecting part of the segments and expand Yamada's approximation method proposed in [7], [8]. In the segment excluding the connected portion, Yamada's method works the same as that in [7], and it is thus considered that the same sufficiently high approximation accuracy is realized using the proposed method. In [7], it was verified how the joint configuration of a snake robot affects the approximation accuracy. Compared with various configurations, such as the configuration using the universal joint and the configuration including the roll axis joint, it was found that the joint configuration we use in this paper realized the highest approximate accuracy. Additionally, in [7], it was shown that this approximation error was proportional to the -2 power of the number of links per length. We consider that our proposed method maintains sufficient accuracy as long as the constraint condition given in section III–C is satisfied.

IV. GAIT DESIGN

We design two novel gaits for the snake robot using the representation method presented in Section III. In the design of these gaits, we use only simple shapes, namely a straight line, a circular arc, and a helix.

A. Moving over a Flange on a Pipe

A snake robot moving on a cylindrical obstacle is expected to relate to the inspection of a pipe or a search or monitoring task performed by climbing a tree or street lamp. Rollinson and Choset [4] realized autonomous compliance control of a snake robot moving on a pipe whose diameter varies continuously. Because their method does not lift the body of the snake robot locally, it can not be applied for a snake robot to cross obstacles like flanges, where the pipe diameter changes greatly discontinuously. Vespignani et al. [13] proposed a method for rolling on a horizontal pipe with flanges. However, their method needs an elastic element in the mechanism of robot. Additionally, there is no control that maintains the gripping force when the snake robot passes over the flange and the method cannot be applied to motion along a vertical pipe. In this paper, we propose a novel gait that allows the snake robot to climb over a flange on a pipe, even in the case that the pipe is vertical.

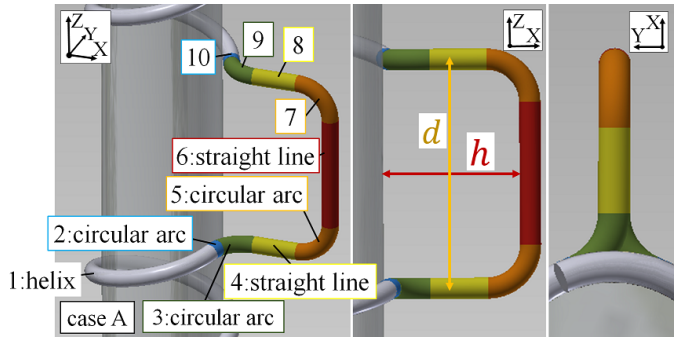

Fig. 5. Overview of the form in case A.

TABLE II
PARAMETERS OF SEGMENTS FOR THE MOTION OF CLIMBING OVER A FLANGE

seg no. j	shape	parameter	$\hat{\psi}_j$
10m+1	helix	$(a_j, b_j, \phi_j) = (r_\mathrm{h}, p_\mathrm{h}/(2\pi), \phi_\mathrm{h})$	$-\pi/2$
10m+2	circular arc	$(r_j, \phi_j) = (r_c, \alpha_\mathrm{h})$	$-\pi/2$
10m+3	circular arc	$(r_j, \phi_j) = (r_c, \beta)$	0
10m+4	straight line	$l_j = l_\mathrm{s}$	$-\pi/2$
10m+5	circular arc	$(r_j, \phi_j) = (r_c, \pi/2)$	0
10m+6	straight line	$l_j = d - 2r_c$	γ
10m+7	circular arc	$(r_j, \phi_j) = (r_c, \pi/2)$	0
10m+8	straight line	$l_j = l_s$	$\pi/2$
10m+9	circular arc	$(r_j, \phi_j) = (r_c, \beta)$	$\pi/2$
10m+10	circular arc	$(r_j, \phi_j) = (r_c, \alpha_\mathrm{h})$	$\pi/2$

1) Design of a Segment Shape: It is possible for a snake robot to propel itself along a pipe through *helical rolling* [10], [11]. In the case of our proposed gait, the *bridge part* is provided in the middle of a helix for striding over obstacles. The shape of the bridge part is determined by specifying the height and width as described later. The segment configuration of this form is divided into two cases, A and B, depending on the height of the bridge part. The criteria for switching between the two cases are derived later.

We first consider case A. The segment configuration for case A are shown in Fig. 5 and parameters of each segment are determined as given in Table II. The target form is formed by repeatedly connecting these 10 segments, and this unit of segments is called a *segment unit*. $m \in \mathbb{Z}$ in Table II is an index of a segment unit. Fig. 5 shows segment unit 0. Segment 1 is a helix with radius r_h, pitch p_h, and central angle ϕ_h. This helix must be long enough to cover the whole body of the robot:

$$(n_\mathrm{joint}+1)l \;\le\; l_1 \;=\; \phi_\mathrm{h}\sqrt{r_\mathrm{h}^2 + \left(\frac{p_\mathrm{h}}{2\pi}\right)^2}. \tag{11}$$

Pairs of segments, namely segments 2 and 10, segments 3 and 9, segments 4 and 8, and segments 5 and 7, have the same shapes, respectively. Segment 6 is parallel to the axis of the helix, while segments 3, 4, 8, and 9 are on a plane perpendicular to the helix axis. Segments 5 and 7 are on the same or another plane parallel to the helix axis.

The radius of all circular arcs is denoted r_c. The height h of the bridge part is the distance between the cylinder and segment 6, and the width d is the distance between segments 4 and 8. r_h, h, and d depend on the environment, while p_h and r_c are decided by an operator. Segments 4, 6, and 8 constitute a straight line with a length of zero or more, and satisfy the relationship $d \ge 2r_\mathrm{c}$.

The central angle α of segments 2 and 10, central angle β of segments 3 and 9, twist angle γ between segments 6 and 7, and length l_s of segments 4 and 8 are derived from the geometry. Segments 2 and 10 constitute a circular arc that changes the direction so that it is perpendicular to the axis of the helix by canceling the inclination of the helix. The diagram on the left of Fig. 6 shows the projection of segment 1, 2 and a cylinder onto a plane. O_2 represents the center of the circular arc in segment 2. When the slope angle of the tangent of the helix is α_h, the central angle of segment 2 is determined as α_h.

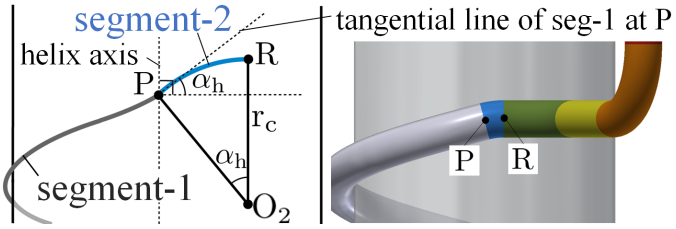

Fig. 6. Diagram of segment 2

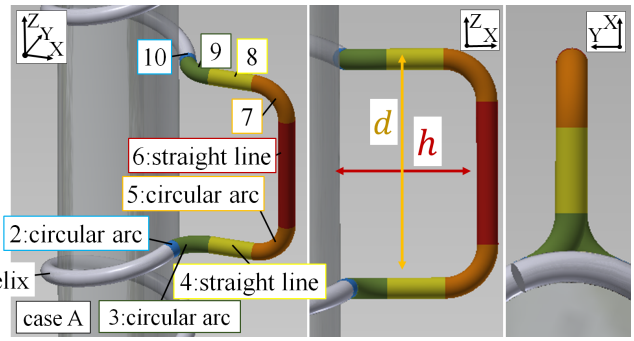

Fig. 7. Diagram of segments 1 to 5 in case A.

The diagram on the left of Fig. 7 shows the projection of segments 1 to 5 onto a plane perpendicular to the axis of the helix. O_h is the intersection point of the plane and the axis of the helix. Line segments PR and UV are projections of segments 2 and 5, respectively, while arc PS is the projection of a part of the segment 1. O_c is the center of the arc of segment 3. Points O_h, S, T, U, and V are on the same straight line. From Fig. 7, β, l_s, and γ are determined according to

$$\begin{aligned}
\beta &= \angle \mathrm{O_hO_cT} - \angle \mathrm{O_hO_cR} \\
&= \arccos\left(\frac{r_\mathrm{c}}{\sqrt{(r_\mathrm{h}+r_\mathrm{c})^2 + (r_\mathrm{c}\sin\alpha_\mathrm{h})^2}}\right) \\
&\quad - \arctan\left(\frac{r_\mathrm{c}\sin\alpha_\mathrm{h}}{r_\mathrm{h}+r_\mathrm{c}}\right) \qquad (12)\\
l_\mathrm{s} &= h - \mathrm{ST} - \mathrm{UV} \\
&= h - \sqrt{(r_\mathrm{c}\sin\alpha_\mathrm{h})^2 + 2r_\mathrm{h}r_\mathrm{c} + r_\mathrm{h}^2} + r_\mathrm{h} - r_\mathrm{c} \qquad (13)\\
\gamma &= 0. \qquad (14)
\end{aligned}$$

The value of h in case $l_\mathrm{s} = 0$ is the border value between cases A and B. From (13), the border height h_b is derived as

$$h_\mathrm{b} = \sqrt{(r_\mathrm{c}\sin\alpha_\mathrm{h})^2 + 2r_\mathrm{h}r_\mathrm{c} + r_\mathrm{h}^2} - r_\mathrm{h} + r_\mathrm{c}. \tag{15}$$

The case with $h > h_\mathrm{b}$ is case A.

The target form in case B ($h \le h_\mathrm{b}$) is shown in the left side of Fig. 8. The lengths l_s of segments 4 and 8 are zero. The middle of Fig. 8 shows the projection of segments 1 to 5 onto a plane perpendicular to axis of the helix, as in Fig. 7. β and γ are obtained from a different geometric relationship as in case A. When $\beta = 0$, h has the lower limit h_min:

$$h_\mathrm{min} = \sqrt{r_\mathrm{h}^2 + r_\mathrm{c}^2(1+\sin\alpha_\mathrm{h})^2} - r_\mathrm{h}. \tag{16}$$

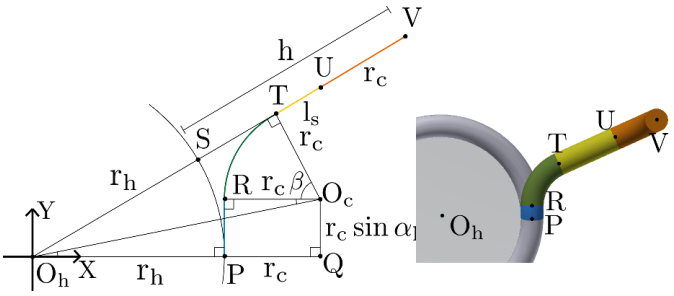

Fig. 8. Diagram of segments in case B.

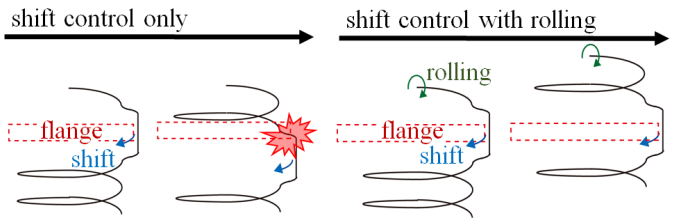

Fig. 9. Movement over a flange. Left: Shift control only leads to the robot colliding with the flange. Right: Combined rolling with shift control avoids a collision.

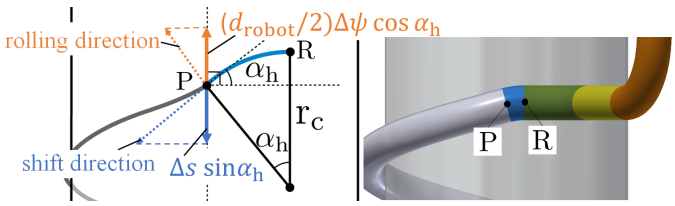

Fig. 10. Relationship between Δs and $\Delta\psi$

The shape of the bridge part is determined by the height h and width d satisfying $h_{\min} \leq h$ and $2r_{\mathrm{c}} \leq d$.

The minimum length of the snake robot is the sum of the length of the bridge-part and the length of the head-side part and the tail-side part winding around the pipe in a helical form. In order to prevent the fall, the required length of the helical parts is related to the friction between the snake robot and the environment and the torque of the motor, so it is difficult to analytically obtain it, which is a future task.

2) Combining Shift Control and Rolling: As shown at the left of Fig. 9, when executing only shift control, the position of the bridge part relative to the flange is not constant and the robot collides with the flange. As shown at the right of Fig. 9, rolling motion should be carried out while executing shift control to keep the bridge part across the flange when the snake robot passes over the flange. The relationship between the shift length Δs and the change in the bridge part is shown in Fig. 10. As the rolling distance is given by $\Delta\psi d_{\mathrm{robot}}/2$. Δs and rotation angle $\Delta\psi$ must satisfy the relation

$$\Delta\psi(\frac{d_{\mathrm{robot}}}{2})\cos\alpha_{\mathrm{h}} = -\Delta s \sin\alpha_{\mathrm{h}}, \tag{17}$$

where d_{robot} is the diameter of the body of the snake robot.

B. Crawler gait

We proposed the *crawler gait*, which has higher adaptability to uneven ground because the snake robot behaves like a crawler belt, similar to the *loop gait* in [14], [15]. Furthermore, this gait does not require a special mechanism to connect the two ends of the robot such like the loop gait. Because more than one part of the snake robot is grounded, the crawler gait has greater stability. The crawler gait can be regarded as modifying the shape of the wave in *3D pedal wave* [16]. The *basic form* of the crawler gait for omni-directional motion, *turning form* for turning, and recovery motion in the event of a fall are explained.

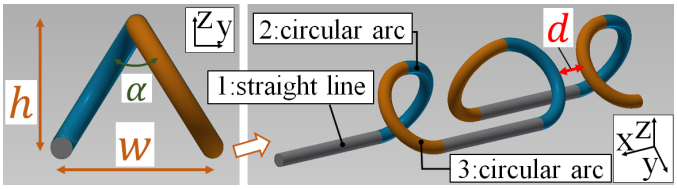

Fig. 11. Segment configuration of the basic form of the crawler gait.

TABLE III
PARAMETERS OF SEGMENTS FOR THE BASIC FORM OF THE CRAWLER GAIT

seg no. j	shape	parameter	$\hat{\psi}_j$
$6m+1$	straight line	$l_j = 2r_{\mathrm{c}} + d$	0
$6m+2$	circular arc	$(r_j, \phi_j) = (r_{\mathrm{c}}, \pi)$	α
$6m+3$	circular arc	$(r_j, \phi_j) = (r_{\mathrm{c}}, \pi)$	0
$6m+4$	straight line	$l_j = 2r_{\mathrm{c}} + d$	0
$6m+5$	circular arc	$(r_j, \phi_j) = (r_{\mathrm{c}}, \pi)$	$-\alpha$
$6m+6$	circular arc	$(r_j, \phi_j) = (r_{\mathrm{c}}, \pi)$	0

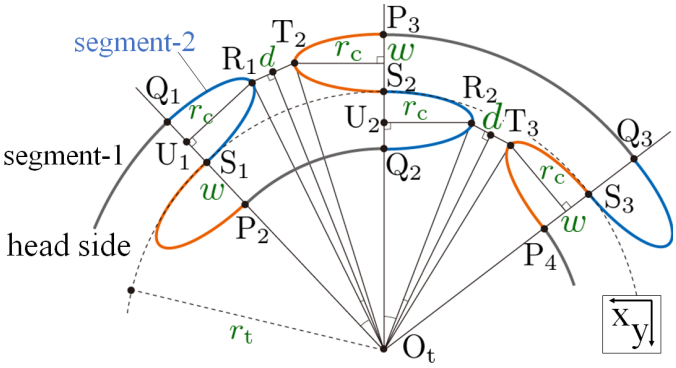

Fig. 12. Schema of the turning form of the crawler gait.

1) Basic Form: The segment configuration of the *crawler-gait basic form* is shown in Fig. 11. This form is designed by repeatedly connecting units consisting of six segments. The straight line segments touch the ground whereas the circular arc segments are floating. By setting three form parameters, namely the height h, width w, and margin of the distance between the circular arcs d, the target form is determined as given in Table III. $m \in \mathbb{Z}$ is the index of a segment unit. r_{c} is the radius of circular arcs and α is the twist angle between circular arcs. These are obtained as

$$r_{\mathrm{c}} = \frac{\sqrt{h^2 + \left(\frac{w}{2}\right)^2}}{2}, \tag{18}$$

$$\alpha = 2\arctan\left(\frac{w}{2h}\right). \tag{19}$$

Shift control and rolling generate propulsion in the x and y direction in Fig. 11, respectively. So, it is capable of omni-directional movement.

2) Turning Form: By changing the straight line segment in the basic form to appropriate circular arc segments, a snake robot is able to turn. In this *turning form*, the turning curvature $\kappa_{\mathrm{t}} \neq 0$ is added to the form parameter in addition to h, w, and d of the basic form. κ_{t} has a positive value when the snake robot turns its head to the left and a negative value when it turns to the right. Fig. 12 is the schema of the turning form. r_{c} and α are the same as those for the basic

TABLE IV
PARAMETERS OF SEGMENTS COMPOSING THE TURNING FORM OF THE CRAWLER GAIT.

seg no. j	shape	parameter	$\hat{\psi}_j$
$6m+1$	circular arc	$(r_j, \phi_j) = (r_\mathrm{r}, \phi_\mathrm{r})$	$-\beta_\mathrm{r}$
$6m+2$	circular arc	$(r_j, \phi_j) = (r_\mathrm{c}, \pi)$	α
$6m+3$	circular arc	$(r_j, \phi_j) = (r_\mathrm{c}, \pi)$	β_l
$6m+4$	circular arc	$(r_j, \phi_j) = (r_\mathrm{l}, \phi_\mathrm{l})$	$-\beta_\mathrm{l}$
$6m+5$	circular arc	$(r_j, \phi_j) = (r_\mathrm{c}, \pi)$	$-\alpha$
$6m+6$	circular arc	$(r_j, \phi_j) = (r_\mathrm{c}, \pi)$	β_r

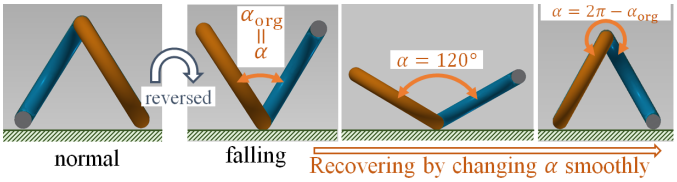

Fig. 13. Recovery motion of the crawler gait.

shape and can be obtained from (18) and (19) respectively. $\mathrm{O_t}$ is the center of the arc $\mathrm{P}_k\mathrm{Q}_k (k \in \mathbb{Z})$. r_t is the turning radius defined as $r_\mathrm{t} = \mathrm{O_tS}_k = 1/|\kappa_\mathrm{t}|$. The parameters of each segment are defined in Table IV. Fig. 12 is the projection of segments onto a xy–plane. From Fig. 12, r_r, ϕ_r, r_l, ϕ_l, β_r, and β_l can be obtained according to

$$(r_\mathrm{r}, \quad \phi_\mathrm{r}) = (\overline{\mathrm{O_tP}_k}, \quad \angle \mathrm{P}_k\mathrm{O_tQ}_k) \ (k\text{: odd}), \tag{20}$$
$$(r_\mathrm{l}, \quad \phi_\mathrm{l}) = (\overline{\mathrm{O_tP}_k}, \quad \angle \mathrm{P}_k\mathrm{O_tQ}_k) \ (k\text{: even}), \tag{21}$$
$$\beta_\mathrm{r} = -\frac{\alpha}{2} + \mathrm{sgn}(\kappa_\mathrm{t})\frac{\pi}{2}, \tag{22}$$
$$\beta_\mathrm{l} = \frac{\alpha}{2} + \mathrm{sgn}(\kappa_\mathrm{t})\frac{\pi}{2}, \tag{23}$$

where

$$\overline{\mathrm{O_tP}_k} = r_\mathrm{t} + (-1)^{k+1}\mathrm{sgn}(\kappa_\mathrm{t})\frac{w}{2}, \tag{24}$$
$$\overline{\mathrm{O_tU}_{k-1}} = r_\mathrm{t} + (-1)^{k}\mathrm{sgn}(\kappa_\mathrm{t})\frac{w}{4}, \tag{25}$$
$$\angle \mathrm{P}_k\mathrm{O_tQ}_k = 2\arctan\left(\frac{r_\mathrm{c}}{\overline{\mathrm{O_tU}_{k-1}}}\right) + 2\arcsin\left(\frac{d}{2\sqrt{\overline{\mathrm{O_tU}_{k-1}}^2 + r_\mathrm{c}^2}}\right). \tag{26}$$

It is possible to turn the snake robot by performing shift control with this form. However, there is a problem with this turning motion. In the proposed turning form, it is ideal that segments $(6m+1)$ and $(6m+4)$, which are in contact with the ground, follow concentric circular trajectories of different radii r_r and r_l, respectively. However, because the two segments have the same propulsion velocity generated by shift control, it is necessary for the segments to slip against the ground to follow trajectories of different lengths, and it is thus not possible to accurately realize the trajectory of the turning curvature κ_t.

3) Recovery from Overturning: There is a possibility of the snake robot falling over when moving on rough terrain. Falling while employing the crawler gait is a state in which the circular arc segments that should not be grounded are grounded as shown on the left side of Fig. 13. In this case, it is possible to turn the whole form falling with a hinge-like action by changing α smoothly as shown in Fig. 13, so that the snake robot can return to a state capable of propulsion. The parameter α in (19) is redefined as

$$\alpha = (1-\gamma)\alpha_\mathrm{org} + \gamma(2\pi - \alpha_\mathrm{org}), \tag{27}$$

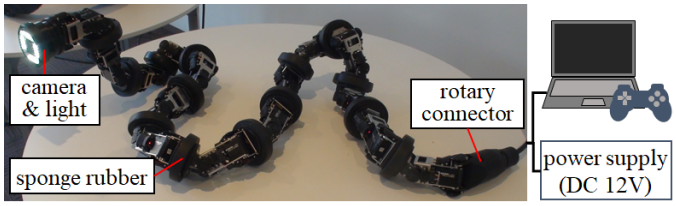

Fig. 14. Experimental system.

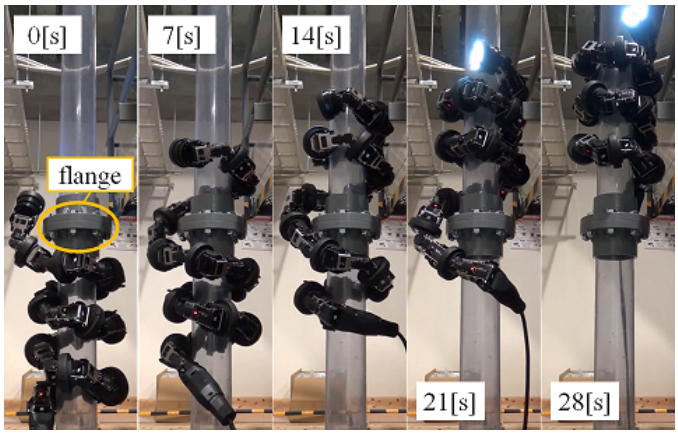

Fig. 15. Experimental result of moving over a flange on a pipe.

where $\alpha_\mathrm{org} = 2\arctan(w/2h)$ and $0 \leq \gamma \leq 1$. By smoothly changing γ from 0 to 1, recovery motion can be performed as in Fig. 13.

V. EXPERIMENT

Experiments were performed to verify the effectiveness of the proposed gaits. The configuration of the developed system is shown in Fig. 14. The snake robot had a module configuration in which one module was composed of two links with a pitch axis joint and a yaw axis joint. The snake robot also has a wireless camera and a light. The length of each link was 80 mm, the diameter of the thickest part of the module was 100 mm, and the weight of one module was about 0.5 kg. The maximum continuous torque of joint motors was 4.0 Nm. The robot was composed of 30 joints. The snake robot was powered with a cable, and the target angle of each joint was sent from a computer on the operator side. The cable is connected to the snake robot with a rotary connector that is able to rotate infinitely while passing power and the signal. It was possible to obtain robot information such as the joint angle and motor current. The sampling time for updating the target joint angle was 20 ms. The operator could perform operations with a gamepad.

A. Moving over a Flange on a Pipe

We carried out an experiment in which the snake robot climbed over a flange on a vertical pipe, a horizontal pipe, and a pipe inclined at 45 degrees. The outside diameter of the pipe was about 110 mm, the outside diameter of the flange was 210 mm, and the thickness of the flange was 44 mm. In the experiment, the operator directly looked at and operated the snake robot. The snake robot was able to move over the flange on the all pipes. Fig. 15 shows the snake robot climbing over the flange from below to above the flange, while a video showing the snake robot moving over the flange is provided in the first multimedia extension Extension1-moving-over-a-flange.mp4. An elastic material was attached to the body of the robot. By making the diameter of the helix segment slightly smaller

than the value for just winding around the pipe, it was possible to push the elastic material against the pipe and exert sufficient gripping force. A similar method has been used when propelling a snake robot outside a pipe with helical rolling in [4]. Proposal of a method for generating a strong tightening force while maintaining the target form to move on a slippery pipe is a future task. The operator adjusted the form parameters d and h of the bridge part according to the shape of the flange and aligned the positions of the bridge part and the flange. If the relative positions of the flange and bridge part were appropriate, motion over the flange proceeded semi-automatically by performing shift control and rolling according to (17). In the experiment, when slippage between the snake robot and the pipe occured and the position relative to the flange shifted, the relative position was adjusted with rolling motion by operator's command.

In physical simulation, the pipe diameter was changed to 150 mm, it can move over the flange. However, the application limit depends on the specification of the robot, such as the length of the body and maximum joint torque. If the diameter of a pipe gets larger, a large joint torque is required. It is the future task to clarify the relationship between the robot specification and the applicable environment.

B. Crawler gait

1) Basic Motion: We carried out experiments on basic motions of the crawler gait, namely propulsion forward and backward, propulsion to the left and right, turning, and recovering from a fall. Results are shown in the second multimedia extension Extension2-crawler-gait-basic-motion.mp4. The form parameters of the crawler gait were $w = 250$ mm, $h = 200$ mm, and $d = 200$ mm.

The snake robot could move back and forward by shifting s_{h}, and move sideweys by changing $\psi(0)$. By performing shift control and rolling at the same time, it is possible to propel the snake robot diagonally.

Turning by shift control with turning form is shown in the video. The target turning radius r_{t} was $500\mathrm{mm}$, but it seemed that the robot was slipping against the floor, and the actual turning radius was larger than the target. Although the length of the target trajectory differed between the inner side and outer side of the grounded arc segment, the same propulsion velocity was generated by the shift control, resulting in the above problem. Furthermore, because of the difference in lengths of the inner and outer arc segments, there was a difference in the frictional force and the slipping was not constant depending on the contact condition of the segments. Improvement of the turning motion is a future task.

Experiments for recovery motion were carried out on the floor and the step field. The snake robot was artificially turned over into a falling state from the usual state in which the crawler gait propelled the snake robot. Starting from this overturned state, we performed recovery motion by smoothly changing α from 0 to 1 using (27), and we succeeded in recovering to the state in which the snake robot can be propelled. Investigation of a method that can be used to recover in various situations is a future task.

It is difficult to operate using the camera image when moving with the crawler gait because the direction of the camera is very oscillatory. Establishing a method of stabilizing the posture of the mounted camera is a future task.

2) Movement on Rough Terrain: Two experiments were conducted in which the snake robot moved across rough terrain with the crawler gait. One experiment was conducted on a debris field while the other on a step field. The appearance of these experiments are shown in Fig. 16 and Fig. 17, and details are shown in the third multimedia extension Extension3–crawler-gait-rough-terrain.mp4.

The debris field was made by randomly laying wooden pieces and sponges of various shapes. The experiment was performed using the snake robot covered with cloth that protected against dust. Note that the operator commanded the snake robot simply to propel forward with shift control and did not use any information on the environment, and yet the robot was able to move across the debris field adaptively.

Fig. 16. Experimental result of the movement on a debris field

Fig. 17. Experimental result of the movement on a step field

In the experiments conducted on the step field, we use the 32-joint snake robot. The height of one step in the step field was 100 mm. In this experiment, the operator appropriately commanded the snake robot to propel itself forward or to turn, so that it moved over the step field. The joint angle did not necessarily match the target because the control of the joint angle of the robot was the position control within the limitation of torque. This property generated compliant motion and realized adaptation to the shape of the environment.

VI. Conclusion

We proposed a method of designing the target form of a snake robot by connecting curve segments having known characteristics. In addition to simple shapes, such as a straight line, a circular arc, and a helix, any shape can be used for the connected curve segments as long as the curvature and torsion are calculated analytically. We also derived shape constraints such that the target joint angle does not exceed the range of motion of joint angle of the snake robot.

Furthermore, using this method, we proposed two novel gaits that allow the snake robot to move in a complex environment. One gait is for motion over obstacles on a pipe that change in diameter discontinuously, like a flange, and the other gait is the *crawler gait* aimed for motion across rough terrain. Even with the complicated target form as a whole, we could easily determine the shape of each segment using geometric calculation. We carried out experiments to verify the effectiveness of each gait and realized movement over a flange, the basic motion of the crawler gait, and movement over a debris field and step field with the crawler gait.

If it is possible to easily design a form suitable for various complicated environments, the applicable fields of the snake robot are extended. It is necessary to make it easier to design complicated target forms by increasing the types of curve segments. Additionally the kinematic/dynamic analysis of the proposed gait is left as a future task. Carrying out the comparison with other gaits is also an important task remain. With regard to the crawler gait, a goal is for the snake robot to move on varying rough terrain freely by improving this gait. For these purposes, it is necessary to increase mobility of the crawler gait by adapting to the terrain shape and to propose a control method for trajectory tracking. And realizing autonomous movement by installing various sensors to obtain information about the environment is also important.

References

[1] M. Saito, M. Fukaya, and T. Iwasaki, "Serpentine Locomotion with Robotic Snakes," *IEEE Control Syst.*, vol. 22, no. 1, pp. 64–81, Feb. 2002.

[2] F. Matsuno and K.Mogi, "Redundancy Controllable System and Control of Snake Robot Based on Kinematic Model," *Proc. IEEE Conf. Decision and Control*, 2000, pp. 4791–4796.

[3] M. Tesch, K. Lipkin, I. Brown, R. Hatton, A. Peck, J. Rembisz, and H. Choset, "Parameterized and Scripted Gaits for Modular Snake Robots," *Advanced Robotics*, vol. 23, no. 9, pp. 1131–1158, 2009.

[4] D. Rollinson and H. Choset, "Pipe Network Locomotion with a Snake Robot," *Journal of Field Robotics*, vol. 33, no. 3, pp. 322—336, 2016.

[5] G. S. Chirikjian and J. W. Burdick, "The Kinematics of Hyper-Redundant Robot Locomotion," *IEEE Trans. Robot. Autom.*, vol. 11, no. 6, pp. 781–793, Dec. 1995.

[6] S. B. Andersson, "Discretization of a Continuous Curve," *IEEE Trans. on Robotics*, vol. 24, no. 2, pp. 456–461, 2008.

[7] H. Yamada and S. Hirose, "Study of Active Cord Mechanism — Approximations to Continuous Curves of a Multi-joint Body—," *J. of the Robotics Society of Japan*, vol.26, no.1, pp.110–120, 2008. (in Japanese with English Summary)

[8] H. Yamada and S. Hirose, "Study on the 3D Shape of Active Cord Mechanism," *Proc. IEEE Int. Conf. on Robotics and Automation*, 2006, pp. 2890–2895.

[9] H. Yamada, S. Takaoka, and S. Hirose, "A snake-like robot for real-world inspection applications (the design and control of a practical active cord mechanism)," *Advanced Robotics*, vol.27, no. 1, pp.47-60, 2013.

[10] T. Kamegawa, T. Baba, and A. Gofuku, "V-shift control for snake robot moving the inside of a pipe with helical rolling motion," *Proc. IEEE Int. Symp. on Safety, Security, and Rescue Robotics*, 2011, pp. 1–6.

[11] W. Zhen, C. Gong, and H. Choset, "Modeling Rolling Gaits of A Snake Robot," *Proc. IEEE Int. Conf. on Robotics and Automation*, 2015, pp. 3741–3746.

[12] T. Takemori, M. Tanaka, and F. Matsuno, "Gait Design of a Snake Robot by Connecting Simple Shapes," *Proc. IEEE Int. Symp. Safety, Security Rescue Robot.*, 2016.

[13] M. Vespignani, K. Melo, M. Mutlu, and A. J. Ijspeert "Compliant snake robot locomotion on horizontal pipes," *Proc. IEEE Int. Symp. Safety, Security Rescue Robot.*, 2015.

[14] M. Yim, D. G. Duff, and K. D. Roufas , "PolyBot: a Modular Reconfigurable Robot," *Proc. IEEE Int. Conf. on Robotics and Automation*, 2000, pp. 514–520.

[15] T. Ohashi, H. Yamada, and S. Hirose, "Loop forming snake-like robot ACM-R7 and its Serpenoid Oval control," *Proc. IEEE/RSJ Int. Conf. on Intelligent Robots and Systems*, 2010, pp. 413–418.

[16] H. Ohno and S. Hirose, "Design of slim slime robot and its gait of locomotion," *Proc. IEEE/RSJ Int. Conf. on Intelligent Robots and Systems*, 2001, pp. 707–715.